buildings

MDPI

Article

Flexural Behavior of Cross-Laminated Timber Panels with Environmentally Friendly Timber Edge Connections

Honghao Ren *, Alireza Bahrami, Mathias Cehlin and Marita Wallhagen

Department of Building Engineering, Energy Systems and Sustainability Science, Faculty of Engineering and Sustainable Development, University of Gävle, 801 76 Gävle, Sweden; alireza.bahrami@hig.se (A.B.)
* Correspondence: ren.honghao@hig.se

Abstract: As a sustainable construction material, timber is more promoted than steel, concrete, and aluminum nowadays. The building industry benefits from using timber based on several perspectives, including decarbonization, improved energy efficiency, and easier recycling and disposal processes. The cross-laminated timber (CLT) panel is one of the widely utilized engineered wood products in construction for floors, which is an ideal alternative option for replacing reinforced concrete. One single CLT panel has an outstanding flexural behavior. However, CLT cannot be extended independently without external connections, which are normally made of steel. This article proposes two innovative adhesive-free edge connections made of timber, the double surface (DS) and half-lapped (HL) connections. These connections were designed to connect two CLT panels along their weak direction. Parametric studies consisting of twenty models were conducted on the proposed edge connections to investigate the effects of different factors and the flexural behavior of CLT panels with these edge connections under a four-point bending test. Numerical simulations of all the models were done in the current study by using ABAQUS 2022. Furthermore, the employed material properties and other relevant inputs (VUSDFLD subroutines, time steps, meshes, etc.) of the numerical models were validated through existing experiments. The results demonstrated that the maximum and minimum load capacities among the studied models were 6.23 kN and 0.35 kN, respectively. The load–displacement responses, strain, stress, and defection distributions were collected and analyzed, as well as their failure modes. It was revealed that the CLT panels' load capacity was distinctly improved due to the increment of the connectors' number (55.05%) and horizontal length (80.81%), which also reinforced the stability. Based on the findings, it was indicated that adhesive-free timber connections could be used for CLT panels in buildings and replace traditional construction materials, having profound potential for improving buildings' sustainability and energy efficiency.

Keywords: cross-laminated timber; adhesive-free edge connection; load capacity; finite element method; flexural behavior; VUSDFLD subroutine

Citation: Ren, H.; Bahrami, A.; Cehlin, M.; Wallhagen, M. Flexural Behavior of Cross-Laminated Timber Panels with Environmentally Friendly Timber Edge Connections. *Buildings* **2024**, *14*, 1455. https://doi.org/10.3390/buildings14051455

Academic Editor: Sathees Nava

Received: 10 April 2024
Revised: 8 May 2024
Accepted: 10 May 2024
Published: 17 May 2024

1. Introduction

Cross-laminated timber (CLT) has gone through an outstanding development from its origin to its present state, becoming a generally adopted material in the current construction sector. The concept of layered-up wood (engineered wood) existed in the 19th century [1], but the decent development of CLT occurred in the late 20th and early 21st centuries. In the 1970s and 1980s, researchers in Europe, particularly in Austria and Germany, began exploring the potential of large-scale, multi-layered timber panels. The early investigations involved laminating smaller timber elements to enhance their structural stability. This early work laid the foundation for the up-to-date CLT manufacturing process. In the 1990s, the European market started producing large-scale timber panels with three to seven layers of dimensioned lumber. Since then, CLT has become a commercial product. These timber panels exhibited superior strength and stability due to the cross-lamination, enabling them to be used as load-bearing elements in building construction. The widespread

adoption of CLT was further accelerated by advancements in computer-aided design and manufacturing technologies, such as CNC milling systems [2–5]. Since the beginning of the 21st century, CLT has gradually gained global recognition for its sustainability, strength, and dimensional stability [6,7]. Architects and engineers accepted CLT as an alternative to traditional construction materials like steel, aluminum, and concrete, especially in mid- and high-rise buildings. Regarding the comparison of CLT and reinforced concrete (RC) buildings, Bahrami et al. [8–10] numerically conducted the comparisons between the CLT and RC multi-layer buildings based on their load-bearing capacities. The studies included comparisons of the floor system, wall system, and overall building structures, where the CLT and RC structures were tested under the same conditions with the same dimensions as well. The results revealed that the components from the CLT building depicted a greatly lower self-weight than the RC components, such as the wall and floor (86%) and the foundation (31%). With such vast weight gaps, the CLT building still passed the standard controls, such as maximum deflection, fire resistance, and voice insulation. The outcomes proved that CLT is accepted and preferred to be used as a construction material over RC based on its mechanical performance.

Nevertheless, CLT also has limitations as a construction structure, which include the flexibility of extension and connection in all directions, such as the wall-to-wall and wall-to-floor systems. Since CLT structures were applied in construction, the extension of CLT is highly dependent on the external connector or using hybrid materials such as CLT–concrete composites [11–15]. As for the external connectors, those are mostly made from steel or adhesives, such as screws, bolts, self-tap plates, slide-in plates, polyurethane (PUR) adhesives, melamine–urea–formaldehyde (MUF) adhesives, and epoxy [16–23]. These mentioned solutions for extending CLT panels are not preferable based on the angles of environmental and energy efficiency because the production process of metallic materials and adhesives consumes a higher level of energy and emits much more carbon dioxide than that of timber. Meanwhile, the production of commonly used adhesives also emits harmful pollutants such as volatile organic compounds (VOCs) [24,25]. Therefore, scientists strive to develop environmentally friendly materials for the external connectors for CLT structures, such as timber connectors and carpentry joints [26,27]. Baño et al. [28] designed an adhesive-free CLT panel using dovetail-shaped wood to connect the lamella layers. The specimens were tested under four-point bending and showed acceptable mechanical properties, where similar connections were also studied by Ilgin et al. [29]. However, this type of connection requires a tremendous amount of milling work, and the milling area covers almost the entire panel, which seems impractical for large-scale structures. Except for the large-scale connection, the dowelled connection existed decades ago, which is also named 'Brettstapel' [30]. Based on this concept, Structure Craft [31] developed a new type of dowel-laminated timber (dowellam), which can be used for most building components. With a focus on mechanical properties, many researchers attempt to apply and develop dowel-laminated timber with different structural systems, such as CLT, glulam, and lumbers. Vilguts et al. [32] explored the potential use of hardwood dowels as a substitute for steel fasteners in CLT construction, specifically focusing on single shear-plane joints. It was pointed out that hardwood dowel joints had either equal or greater strength and lateral stiffness than wood screws joints, which illustrated the mechanical potential of wood dowel connections. Moreover, Mehra et al. [33,34] and Sotayo et al. [35] both investigated the application of compressed dowelled wood as an adhesive-free connection for timber structures. The former conducted connecting two glulam beams with compressed wood, and the latter studied the adhesive-free CLT connected by compressed dowels. Both studies prove the viable alternative of using compressed wood as an eco-friendly option. However, the study of using the compressed wood dowel as the edge connection for large-scale timber panels is still insufficient to date.

Two innovative adhesive-free timber edge connections were proposed in this study, which were individually used to connect two three-ply CLT panels by their weak direction. The studied connections were assumed to be standard Scots pine and compressed beech.

The current article examines the flexural behavior of the CLT panels that were connected through the proposed connections. Meanwhile, the sub-goals of this investigation include (1) the parameters from the edge connections that influence the connected panel's flexural behavior and (2) the potential of the proposed edge connections replacing the fasteners concerned with adhesives or metallic materials. The investigated parameters include the connections' length, thickness, sectional area, and number and placement of connectors. Twenty parametric models were generated and designed based on the selected factors. Additionally, the developed models were numerically tested by using ABAQUS 2022 under a four-point out-of-plane bending test. The material properties were extracted from an existing experimental test, which also conducted timber connections through the four-point bending test. The extracted data and the built model were numerically validated based on the obtained mechanical results from the experiment tests. The proposed models were numerically simulated and tested while employing the validated variables. Among all the twenty models, the load–displacement diagrams, strain around mid-span, stress distribution, deflection distribution, and failure modes were collected and analyzed.

Research Significance

The goal of this article is to develop the construction sector based on structural integrity, lifetime energy efficiency, and environmental perspectives. By providing and analyzing innovative adhesive-free timber edge connectors for CLT panels, this article promotes the adoption of sustainable material, timber, as the main construction material instead of steel, concrete, or aluminum. The former has a greater potential for decarbonizing the building industry than that of the latter, which is also able to store carbon during its life-long use. Furthermore, the investigation of the adhesive-free edge connection contributes to energy efficiency by potentially minimizing the energy-intensive processes associated with adhesive production in CLT manufacturing. Meanwhile, parts of the environmental and climate issues (e.g., contaminating the soil and the groundwater, and emitting VOCs) are directly related to the production and use of adhesives due to the difficulties of recycling and disposal. Hence, the current study also assists in downsizing the negative climate impact of the construction field.

2. Method and Adhesive-Free Timber Edge Connections

In this section, the employed mechanical properties of the involved materials (the CLT panel and dowel connector), the geometries of the self-developed adhesive-free timber edge connections, and the test method (such as the numerical model's evaluation, validation, and test setup) are illustrated.

2.1. Connected CLT Panels with Innovative Adhesive-Free Timber Edge Connections

There are two proposed adhesive-free edge connections in this study, which are made of standard timber and compressed dowelled wood. The material and mechanical properties of the CLT panel and compressed dowel are presented in Section 2.3, which are the same as the validated numerical model. Those two developed edge connections were designed to connect two CLT panels in their weak directions. The studied CLT panels are composed of three lamella layers with a thickness of 30 mm at each layer. Meanwhile, each lamella layer was made of multiple parallelly placed lumbers with the cross-section dimensions of 120 mm × 30 mm (width × thickness), and the top and bottom layers (longitudinal layers) were perpendicular to the second lamella layer (transverse layer). The first edge connection, the double surface (DS) connection, was composed of two compressed wood dowel connectors (a diameter D of 10 mm and length of 90 mm) and two rectangular lumbers that were extended from the CLT panel's lamella layers (Figure 1). The DS edge connection has a longitudinal length of 240 mm (LC) and a thickness of 30 mm. The CLT panels were connected, beginning by placing the rectangular connectors from one panel into another CLT panel along the horizontal direction. Then, the dowel connectors were vertically inserted into the CLT panels in one row (N), which also fixed the rectangular

connectors. In addition, d presents the distance between the dowel's pith and the end edge of the panel, which is 60 mm.

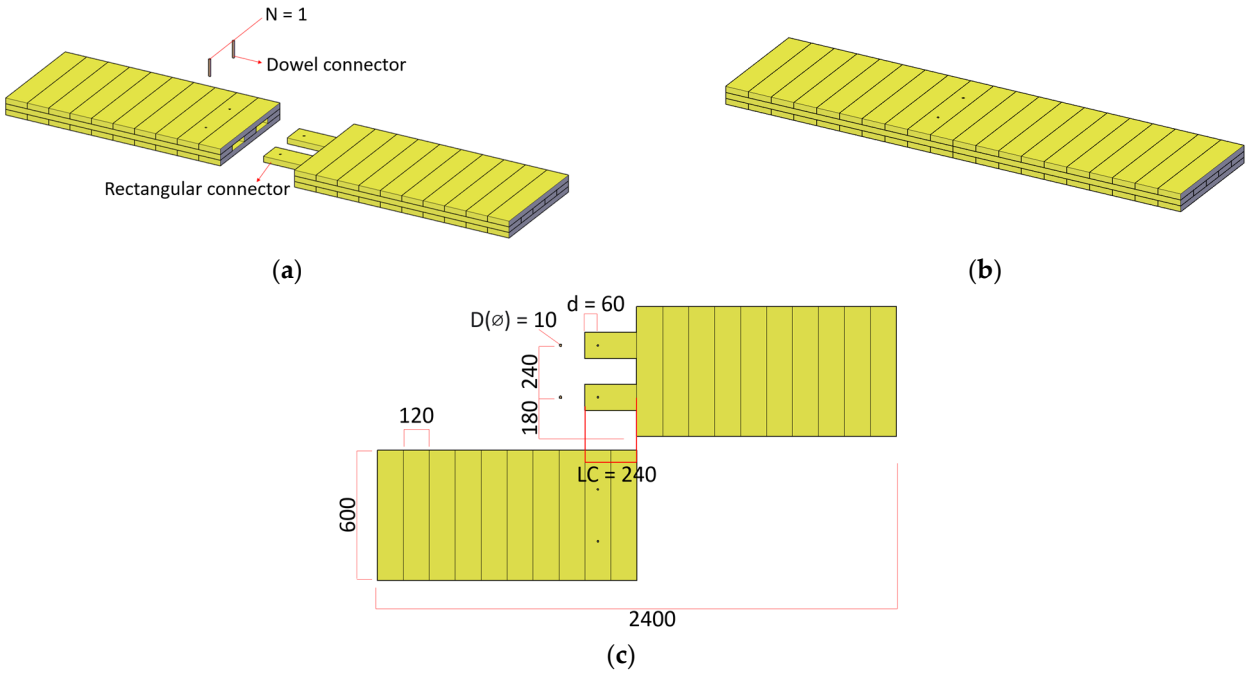

Figure 1. Connected CLT panels using DS edge connection: (**a**) unjointed version, (**b**) jointed version, and (**c**) top view (dimensions are in mm).

Figure 2d exhibits the connected CLT panels using another self-developed adhesive-free edge connection, the half-lapped (HL) connection. In this case, each CLT panel was 50% cut off along its thickness, where the cut-off range was 480 mm × 600 mm (length (LC) × width). After the cut-off modification, two identical CLT panels were placed together, and their cut-off faces were attached. Then, two dowel connectors (with a diameter D of 10 mm and length of 90 mm, compressed wood) were inserted into CLT panels throughout the panel's height, while the dowels were located at the panel's mid-span path with an internal distance of 350 mm. The connected CLT panels with different connections (the DS and the HL edge connections) have the same dimensions of 2400 mm × 600 mm × 90 mm (length × width × thickness). The thickness of the lower panel at the mid-span was 45 mm (TB). The distance between the dowel's pith and the upper panel's edge was 240 mm (d).

2.2. Four-Point Bending Test

Connected CLT panels with the proposed innovative green edge connections were tested under the four-point bending test. The bending test load set was designed following EC 16351 [36] and Eurocode 5 [37], where the distance between the loads is 6 h (h represents the depth) and the distance between the load and support remains at 9 h–12 h (Figure 3c). The specimen was bent in an out-of-plane manner under load F, which was evenly divided by two and symmetrically laid on the top surface. The longitudinal distance between the two-point loads is 540 mm. The load went in the direction that was opposite and parallel to the Y-direction. Likewise, symmetrically positioned supports were situated beneath the connected panels, precisely 45 mm next to the outer edges. The span of the bending test was 2310 mm. The loading process in the numerical models was implemented by displacement control. The applied boundary conditions on both supports were that the displacements on the Y-axis were 0, and the rest of the degrees of freedom on the two supports were not restricted. During the test, the displacement and the reaction force were extracted from the midpoint underneath the connected panel and the load sets, respectively.

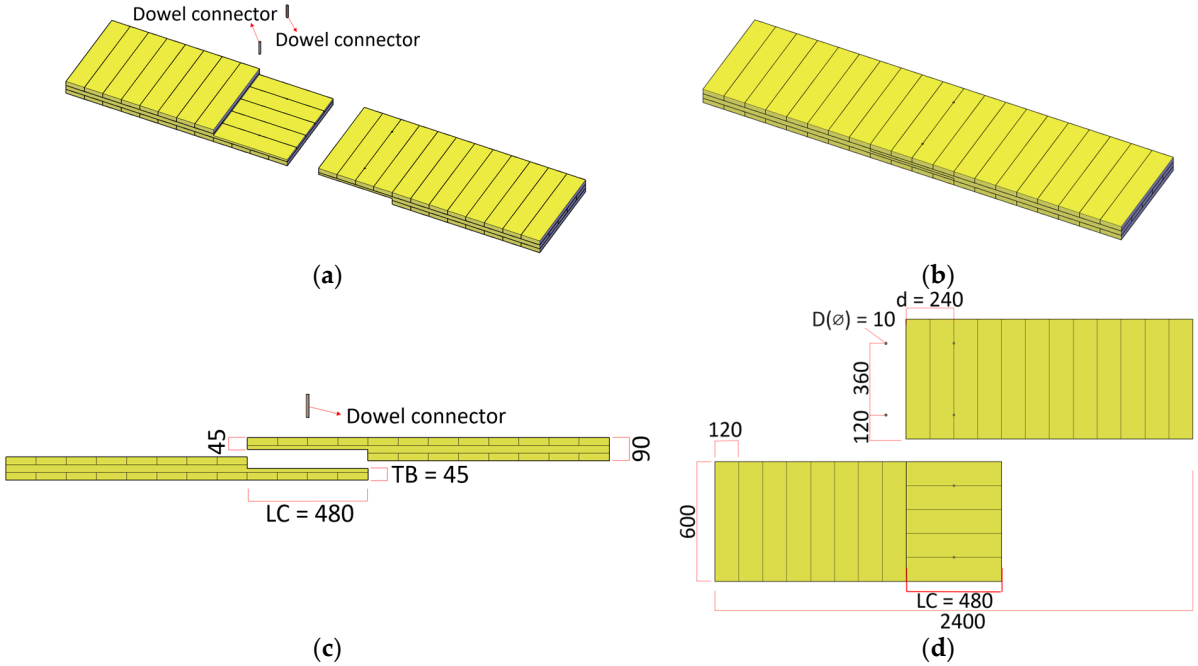

Figure 2. Connected CLT panels using HL edge connection: (**a**) unjointed version, (**b**) jointed version, (**c**) front view, and (**d**) top view (dimensions are in mm).

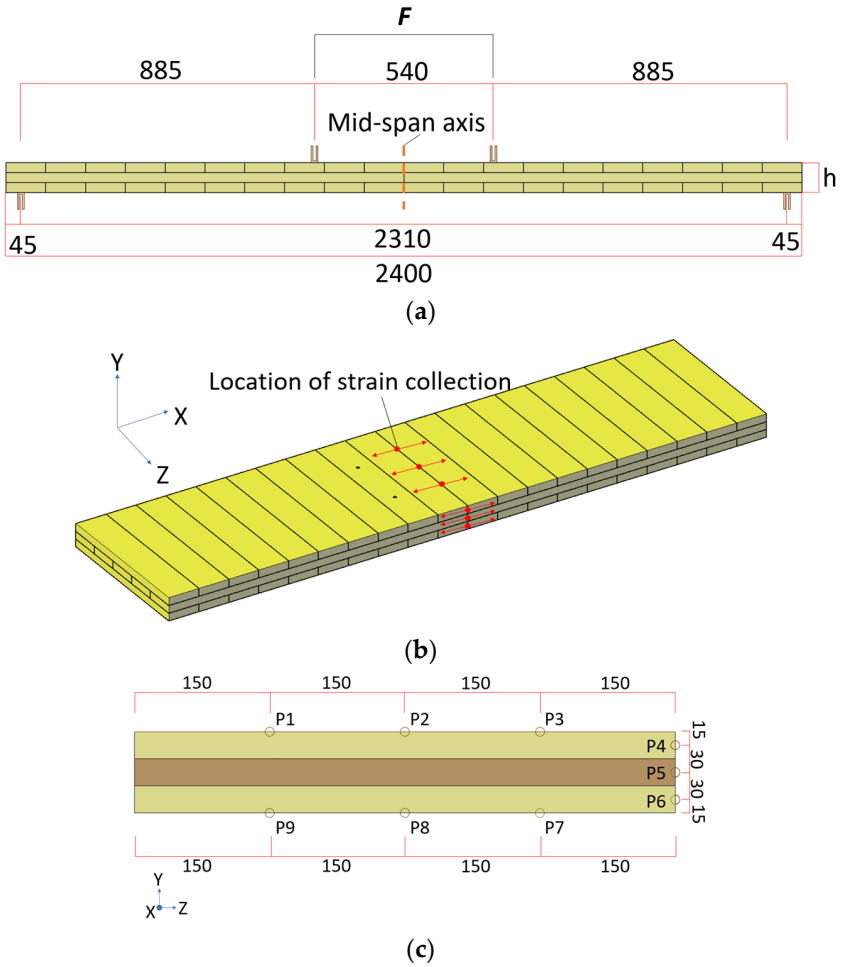

Figure 3. Four-point bending test setup: (**a**) connected panels with boundary conditions, (**b**) location of strain's collection points, and (**c**) section view at panel's mid-span (dimensions are in mm).

2.3. Failures Evaluation and Validation Process of Numerical Model

The numerical model's setup, material properties, and environmental variables were verified by simulating an existing experimental test, which was implemented by Sotayo et al. [35]. As Figure 4 illustrates, the experiment was on an adhesive-free CLT panel with the dimensions of 1500 mm × 600 mm × 60 mm (length × width × thickness). The panel's lamella layers were joined by using the dowel connectors, which were made of compressed beech (diameters of 10 mm and a length of 60 mm). The panel's lamella layers were composed of multiple lumbers with an identical cross-sectional dimension of 115 mm × 20 mm (width × thickness), and the orientations of each lumber are illustrated in Figure 4a. The lumber was made of Scots pine with a mean density of 556 kg/m^3 and moisture contents of 10–15%. According to the experiments, the compressed dowels (beech) have a density of 1300 kg/m^3, an elastic flexural modulus of 25 GPa, moisture contents of 5–8%, and a flexural strength of 269 MPa. The compressed dowels were produced by employing radial compression with a ratio of 54% [33]. The materials of the standard wood and compressed wood from the existing experiment were employed in the numerical simulation for both the validation models and the models with self-developed edge connections. Besides, the mesh size was set to 10 mm after the convergence study (element type: C3D8R, an eight-node linear brick, reduced integration, hourglass control), and the meshed finite element model included 94,920 elements. Furthermore, the numerical analysis was implemented through the static type with the minimum increment size of 5 × 10^{-6}. In the experimental test, the CLT panels without joints were also investigated under a four-point bending test, in which the flexural modulus, strength, and maximum reaction force ranged from 11.1–13.5 GPa, 44.2–55.2 MPa, and 59.8–74.9 kN, respectively. The ratio of the CLT panel's flexural strength with and without the joint is 0.49 (23.6 MPa/48.6 MPa).

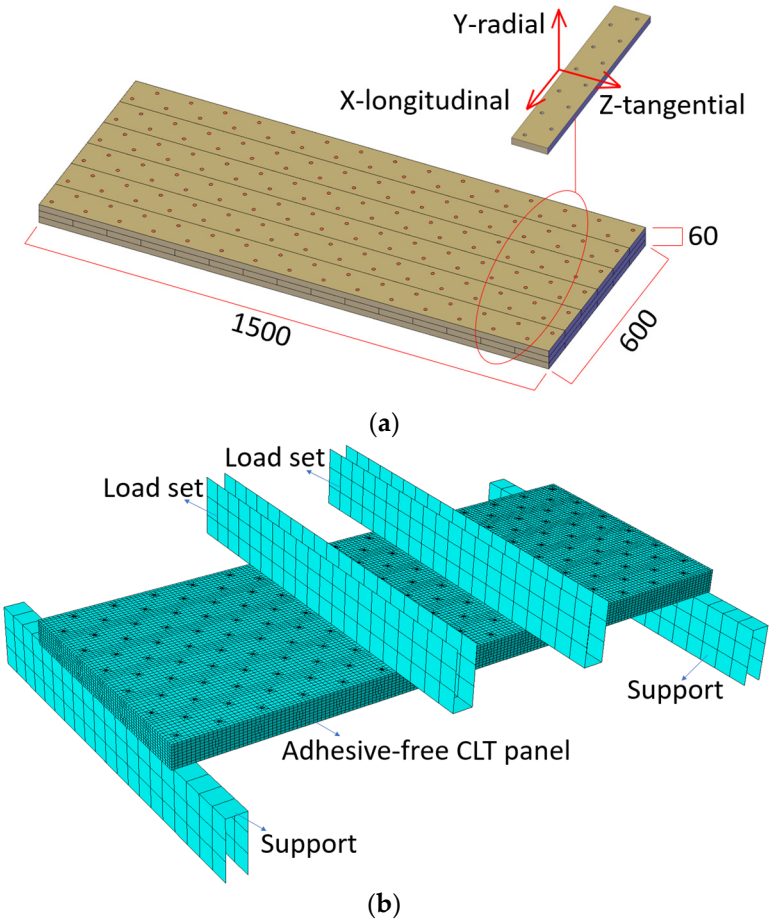

Figure 4. Verification model: (**a**) view and (**b**) assembled finite element model under bending load sets.

The numerical model was considered a self-written VUSDFLD subroutine under an explicit solver in the FEM program, which was used to define the properties of orthotropic materials such as wood. Based on the work of Sitnikova et al. [38] and Gama and Gillespie [39], the studied composite FEM models were assumed to receive instant failure when certain failure criteria were satisfied without accounting for damage evolution. Considering the unidirectional composite failure criteria from Hashin [40], the investigated numerical models employed four failure criteria: the tensile-shear strength and compressive strength of the specimen.

$$f_{1t} = \left(\frac{\sigma_{11}}{S_{1t}}\right)^2 + \left(\frac{\sigma_{12}}{S_{12}}\right)^2 + \left(\frac{\sigma_{31}}{S_{31}}\right)^2 - 1 = 0 \qquad \sigma_{11} > 0 \tag{1}$$

$$f_{2t} = \left(\frac{\sigma_{22}}{S_{2t}}\right)^2 + \left(\frac{\sigma_{12}}{S_{12}}\right)^2 + \left(\frac{\sigma_{23}}{S_{23}}\right)^2 - 1 = 0 \qquad \sigma_{22} > 0 \tag{2}$$

$$f_{1c} = \left(\frac{\sigma_{11}}{S_{1c}}\right)^2 - 1 = 0 \qquad \sigma_{11} < 0 \tag{3}$$

$$f_{2c} = \left(\frac{\sigma_{22}}{S_{2c}}\right)^2 - 1 = 0 \qquad \sigma_{22} < 0 \tag{4}$$

f_{1t} and f_{2t} refer to the tensile-shear failures' evaluations in the longitudinal and tangential directions, respectively. f_{1c} and f_{2c} represent the compressive failures' evaluations in the longitudinal and tangential directions, accordingly. S_{1t} is the axial tensile strength, S_{2t} is the tangential tensile strength, S_{1c} is the axial compressive strength, and S_{2c} is the tangential compressive strength. S_{12}, S_{23}, and S_{31} are the static shear failure strengths. σ means the stress vector, which is related to the material's elastic stiffness C and the strain ε.

In the numerical model, each lumber was created by employing the deformable 3D part, which has the base feature as solid and extrusion. To attach the lumbers within the CLT panel, the cohesive and friction contacts were considered for the lumber's surface, where the implemented friction coefficient was 0.3. The type of cohesive contact was assumed to be traction separation, where the initial interfacial stiffness from the traction (stress)– separation curve was represented by the stiffness coefficients (Table 1). The stiffness coefficient K values refer to the minimum force that can separate two attached surfaces in the normal direction (K_{nn}) and tangential directions (K_{ss} and K_{tt}). The damage nominal stress was also considered in the model, which includes the normal stress (t_{nn}), shear stress (t_{ss}) in the longitudinal direction, and shear stress (t_{tt}) in the lateral direction of the top and bottom surfaces of the interface.

Table 1. Values of traction stiffness coefficients and damage nominal stress.

Contact Property	Stiffness Coefficient			Damage Nominal Stress		
	K_{nn} (N/mm^3)	K_{ss} (N/mm^3)	K_{tt} (N/mm^3)	t_{nn} (N/mm^2)	t_{ss} (N/mm^2)	t_{tt} (N/mm^2)
Values	10^5	10^5	10^5	100	100	100

3. Results and Discussion

This section provides the results and discussion of the proposed green timber edge connections (the DS edge connection and the HL edge connection), which includes the verification and validation of the numerical model, details of the parameter study, the load–displacement curves, load–strain diagrams, strain and deflection distribution, flexural properties, and failure modes.

3.1. Verification and Validation of Numerical Model

According to the experiment test from Sotayo et al. [35], the adhesive-free CLT panel AFCLTP1 was experimentally tested five times with identical test conditions, material, and

specimen geometry. Meanwhile, the load–displacement curves obtained from these five tests performed different elastic and yield behaviors as well as their ultimate moments. Therefore, the results of all five tests, the mean ultimate load, and the mean displacement at failure were all used to validate and verify the developed numerical model. Figure 5 depicts the comparison of the experimental tests and numerical modeling based on their load–displacement diagrams. The average load capacities derived from the five existing experiments, AFCLTP1 (1–5), as well as the developed numerical models, were determined to be 32 kN and 31.96 kN, respectively. The mean rotations associated with the load capacities observed in the AFCLTP1 experiments and numerical models were measured at 85.4 mm and 87.1 mm, respectively. Notably, the numerical model exhibited a slightly lower load capacity (−0.1%) and a greater deflection at failure (1.9%) in comparison to the experimental test. Meanwhile, the elastic and yielding behaviors of the numerical model were relatively close to that of the experiment tests. Consequently, it can be inferred that the numerical model successfully predicted the behavior and load capacity of the beam-to-beam connection with a commendable level of accuracy.

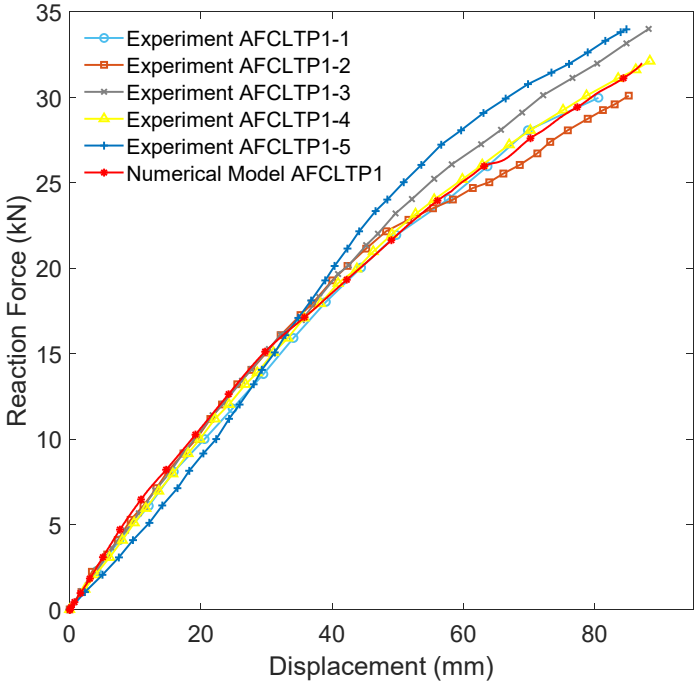

Figure 5. Load–displacement curves of experimental test [35] and numerical study.

3.2. Investigated Parameters of CLT Panels with Self-Developed Adhesive-Free Timber Edge Connections

Based on the proposed two self-developed adhesive-free edge connections (the DS and the HL edge connections), the other eighteen models were generated by modifying different parameters. Therefore, twenty models in total were numerically studied using the validated variables and material properties based on the numerical model AFCLTP1. All the examined parameters are listed in Table 2. The definitions and illustrations of the parameters LC, D, N, d, and TB are provided in Section 2.1. Additionally, 2c means two rows of dowel connectors with a closer distance (Figure 6b) than that of '1-240-10-2-60-1—3', where the distances between the rows of the former and latter were 40 mm and 120 mm. PL expresses the penetrated layers (top layer—transverse layer—bottom layer/1-2-3). DT1 (dowel type 1) is the number of dowels on one row, and DT2 (dowel type 2) is the row number of dowels (Figure 6c). Furthermore, the models involved in the same comparison group belonged to the same parameter's modification. Hence, the original two models ('1-240-10-1-60-1—3' and '2-480-2-1-45-240') were included in all ten comparison groups.

Table 2. Studied parameters of DS and HL edge connections.

Name of Model	Comparison Group	LC (mm)	D (mm)	N	DT1	DT2	TB (mm)	d (mm)	PL
1-240-10-1-60-1—3	1, 2, 3, 4, 5	240	10	1	-	-	-	60	1—3
1-120-10-1-60-1—3	1	120	10	1	-	-	-	60	1—3
1-360-10-1-60-1—3	1	360	10	1	-	-	-	60	1—3
1-240-15-1-60-1—3	2	240	15	1	-	-	-	60	1—3
1-240-20-1-60-1—3	2	240	20	1	-	-	-	60	1—3
1-240-10-2-60-1—3	3	240	10	2	-	-	-	60	1—3
1-240-10-2c-60-1—3	3	240	10	2c	-	-	-	60	1—3
1-240-10-1-180-1—3	4	240	10	1	-	-	-	180	1—3
1-240-10-1-60-1—2	5	240	10	1	-	-	-	60	1—2
1-240-10-1-60-2—3	5	240	10	1	-	-	-	60	2—3
2-480-2-1-45-240	6, 7, 8, 9, 10	480	-	-	2	1	45	240	-
2-240-2-1-45-240	6	240	-	-	2	1	45	240	-
2-720-2-1-45-240	6	720	-	-	2	1	45	240	-
2-480-3-1-45-240	7	480	-	-	3	1	45	240	-
2-480-4-1-45-240	7	480	-	-	4	1	45	240	-
2-480-2-3-45-240	8	480	-	-	2	3	45	240	-
2-480-2-1-30-240	9	480	-	-	2	1	30	240	-
2-480-2-1-60-240	9	480	-	-	2	1	60	240	-
2-480-2-1-45-120	10	480	-	-	2	1	45	120	-
2-480-2-1-45-360	10	480	-	-	2	1	45	360	-

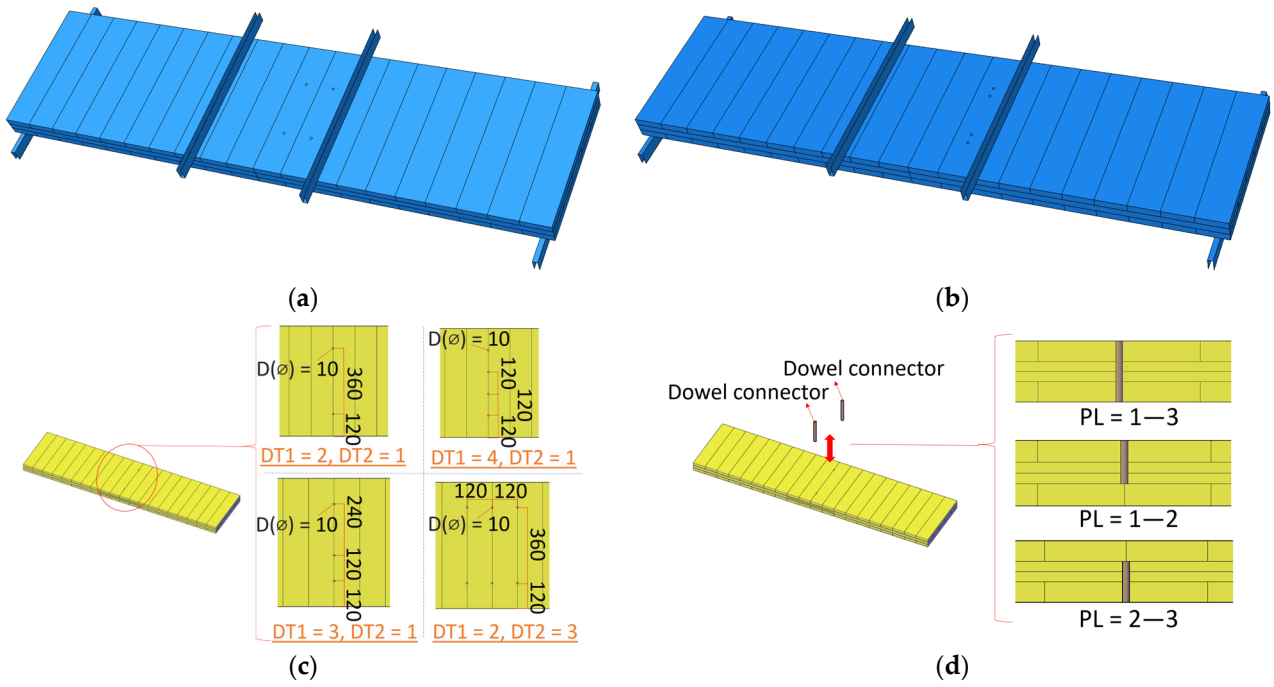

Figure 6. Geometries of: (**a**) models '1-240-10-2-60-1—3', (**b**) models '1-240-10-2c-60-1—3', (**c**) DT1 and DT2, and (**d**) PL.

3.3. Load–Displacement Response

Figure 7 depicts the load–displacement responses of all twenty numerical simulations (under a four-point bending test) based on the parameter study on the original two edge connections: the 'DS edge connection' (1-240-10-1-60-1—3) and the 'HL edge connection' (2-480-2-1-45-240). It was noticed that the ten numerical models based on the DS edge connection showed a fluent and similar linear relationship during its elastic stage under the bending test. It means that the stiffness and elasticity of the DS edge connection were minorly impacted by the studied parameters (the dimensions, placement, and numbers of the connectors). The potential reasons for this phenomenon are as follows: (1) the rectangular connectors majorly bore the moment and the transferred load from the load set, (2) the cross-section dimensions and the materials of the rectangular connector were the same in all the models, and (3) only a limited length of the rectangular connectors nearby the mid-span area were activated for rotational behavior, and the rest part of the rectangular connectors (nearby the dowel connectors) were majorly receiving shear stress. It was observed that most of the numerical models within comparison groups 1–5 performed brittle failures, where the failures were obtained shortly after the load capacities were achieved. This is because the failure of the DS edge connection was initially dependent on the failure of the dowel connector, which received shear force perpendicular to its grain. Therefore, the strength and load capacity among the numerical models of the DS edge connection when it concerns modifications of the dowel connectors. In addition, '1-120-10-1-60-1—3' showed an exceptional ductile failure behavior compared to the other nine models. It indicated that the DS edge connection with a shorter span of the rectangular connector could lead to a high ductility of the connected CLT panel.

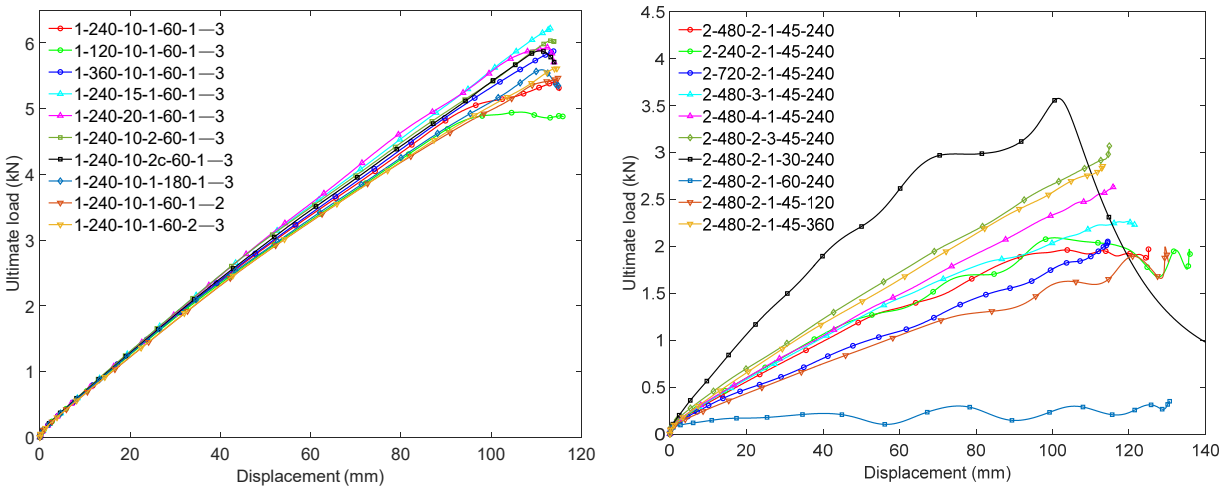

Figure 7. Load–displacement responses: (**a**) comparison groups 1–5 and (**b**) comparison groups 6–10.

Compared to the comparison groups 1–5, the load–displacement responses of comparison groups 6–10 (Figure 7b) exhibited diverse bending elasticities and load capacities. Among the ten numerical models of the HL edge connection, five of them (2-480-2-1-45-240, 2-240-2-1-45-240, 2-480-3-1-45-240, 2-480-2-1-60-240, and 2-480-2-1-45-120) performed ductile failure, while the others failed in a fracture manner. Meanwhile, those ductile-failed models displayed a relatively lower bending strength and elasticity compared to the fracture-failed models. The likely explanation for this outcome is that the HL edge connection's flexural behavior was impacted by the thickness and effective length of the HL joint's upper part, which presented a positive correlation in between. The model '2-480-2-1-60-240' (the thickness of the HL joint's upper part was 30 mm) showed the lowest reaction force compared to others, which was close to 0.5 kN during the entire test. Meanwhile, another model with a 30 mm thicker upper part of the HL joints (2-480-2-1-30-240) presented the

highest ultimate load and stiffness. Therefore, the recommended design thickness of the HL joint's upper part should be at least half of the HL joint's total thickness. Most of the fracture-failed models (2-480-4-1-45-240, 2-480-2-3-45-240, 2-480-2-1-30-240, and 2-480-2-1-45-360) depicted a good linear relationship between the load and displacement, which were also close to each other. It indicated that those four models have higher stability than the others under out-of-plane bending.

The values of the ultimate load and displacement at the failure of all studied numerical models (comparison groups 1–10) are listed in Table 3. It was observed that the load capacity of the DS edge connection (mean value of 5.70 kN) was 149% higher than that of the HL edge connection (mean value of 2.29 kN). This is because the DS edge connection was fixed in the longitudinal direction (by the dowel connectors) and vertical-transverse plane (by the CLT panel) from sliding and global rotation, while the HL edge connection was fixed only in the longitudinal direction (by the dowel connectors). Mehra et al. [33] also evaluated the bending performance of engineered wood (with a length, width, and depth of 3160 mm, 130 mm, and 160 mm, respectively) with a timber connection, which resulted in a mean load capacity of 4.54 kN. The obtained load capacity from Mehra et al. [33] was 20% lower than that of the DS edge connection, while the specimen employed in the current study has greater dimensions. It depicted an improvement in applying the adhesive-free timber connection for CLT panels. Meanwhile, the other CLT panels with hybrid metallic edge connections, in which steel screws and LVL splices were applied, exhibited a relatively higher load capacity of 19.4 kN [17]. However, the volumes of the tested connectors and CLT panels in the current study are far smaller (77%) than those of the CLT panels jointed by hybrid metallic connectors. It showed that the DS connection is as competitive as the hybrid metallic connectors from both mechanical and environmental perspectives.

According to the standard deviations of load capacities of the two edge connections, the DS edge connection's values (0.37) were clustered more tightly around the mean than that of the HL edge connection (0.87). The values of the coefficient of variation also depicted that the DS edge connection had an 82.8% greater level of dispersion around the mean than that of the HL edge connection (0.87). The outcomes indicated that the DS edge connection was more stable than the HL edge connection based on their load capacities. The displacements at the failure of two edge connections also displayed a similar dispersed level around the mean as that of the load capacities. The mean displacement at failure of the DS edge connection (112.49 mm) was 3.5% lower than that of the HL edge connection (116.55 mm), which implied that the HL edge connection had a higher ductility. It was likely because the DS edge connection was more tightly jointed than the HL edge connection due to their geometries.

Table 3. Obtained results from CLT panels numerically tested under four-point bending.

Name of Model	Comparison Group	Ultimate Load (kN)	Difference	Displacement (mm)	Difference
1-240-10-1-60-1—3	1, 2, 3, 4, 5	5.40	-	114.07	-
1-120-10-1-60-1—3	1	4.95	−8.43%	106.52	−6.62%
1-360-10-1-60-1—3	1	5.88	8.80%	113.92	−0.13%
1-240-15-1-60-1—3	2	6.23	15.26%	113.14	−0.81%
1-240-20-1-60-1—3	2	5.93	9.80%	112.46	−1.41%
1-240-10-2-60-1—3	3	6.04	11.71%	113.23	−0.74%
1-240-10-2c-60-1—3	3	5.88	8.83%	110.81	−2.86%
1-240-10-1-180-1—3	4	5.59	3.50%	111.24	−2.48%
1-240-10-1-60-1—2	5	5.47	1.34%	114.91	0.74%
1-240-10-1-60-2—3	5	5.61	3.85%	114.60	0.46%
Mean		5.70		112.49	

Table 3. *Cont.*

Name of Model	Comparison Group	Ultimate Load (kN)	Difference	Displacement (mm)	Difference
Std. Dev.		0.37		2.49	
COV		6.51%		2.24%	
2-480-2-1-45-240	6, 7, 8, 9, 10	1.98	-	125.06	-
2-240-2-1-45-240	6	2.09	5.56%	100.52	−19.62%
2-720-2-1-45-240	6	2.05	3.54%	114.44	−8.49%
2-480-3-1-45-240	7	2.27	14.65%	119.66	−4.32%
2-480-4-1-45-240	7	2.65	33.84%	116.20	−7.08%
2-480-2-3-45-240	8	3.07	55.05%	114.84	−8.17%
2-480-2-1-30-240	9	3.58	80.81%	101.56	−18.79%
2-480-2-1-60-240	9	0.35	−82.32%	130.67	4.49%
2-480-2-1-45-120	10	2.00	1.01%	129.43	3.49%
2-480-2-1-45-360	10	2.86	44.44%	113.12	−9.55%
Mean		2.29		116.55	
Std. Dev.		0.87		10.26	
COV		37.87%		8.81%	

The results of the models from comparison groups 1–5 and 6–10 were compared to their original models 1-240-10-1-60-1—3 and 2-480-2-1-45-240, respectively. The difference ratios were provided as well. It demonstrated that the longitudinal length of the DS edge connection had a significant impact on its load capacity, which was improved up to 8.8% by increasing the connector's length to 360 mm (1-360-10-1-60-1—3) from 240 mm. This is because the rectangular connector with a longer distance bore a higher transferred load before it reached the dowel connector, which was decisive in the failure. Based on the displacements at failure, it was also noticed that the DS joint with a smaller distance also exhibited a higher ductility because the transferred load was activated in a smaller effective area. The results of comparison group 2 demonstrated that the diameter of the dowel connectors had a positive correlation with the load capacity of the DS edge connection, which could be improved up to 15.26% (diameter of 15 mm). Meanwhile, it also showed that the dowel connector with a higher diameter than 15 mm would decrease the ultimate load. The potential reason for this phenomenon is that the dowel connector with a thicker diameter had a higher shear strength against the grain's perpendicular direction as its shear plane's area was larger. Meanwhile, the larger the diameter of the dowel connector was, the smaller the volume of the rectangular connector was. Therefore, the preferred diameter of the dowel element of the DS edge connection was 15 mm, based on its flexural load capacity. According to the results of comparison group 4, the number and placement of the dowel connector have different and clear effects on the connection's flexural behavior, where the former positively affected the performance and the latter exhibited the impact negatively. The DS edge connection with a double number of dowel connectors performed an 11.71% higher load capacity than that of the original model (1-240-10-1-60-1—3), which proved that the dowel connectors played a positive role in effecting the DS connection's bending capacity. Moreover, the placement of the dowel connections also affected the DS connection's performance, where the models with a smaller distance between each dowel connector showed a lower load capacity than that of the model with a larger internal distance between each dowel (about 3%). The explanation for this outcome was that the connection with a greater number of dowel connectors meant a larger area of the shear plane. At the same time, a larger internal distance between the dowels helped to distribute the transferred load on the connector in a more even manner. The load capacity and

displacement at failure from the model '1-240-10-1-180-1—3' (comparison group 4) were close to the original model, with a small difference of 3.5% and −2.48%. It implied that the longitudinal distance between the dowel connector and the edge of the rectangular element did not play a major role in the influence of the DS edge connection's mechanical behavior. This is because the contained dowel connector with different locations in the connection had the same shear plane area of the dowel and rectangular elements, which meant the connection system's shear strength remained the same. A similar phenomenon also occurred in comparison group 5, where the difference ratio between each model in this group was minor (up to 3.85%). It revealed that the different lengths of dowel connectors minorly impacted the DS edge connection's ductility and load capacity. The potential explanation for this result was that the dowel connectors of all comparison models went through the entire transverse layer, which was the decisive part of transferring the longitudinal load.

As for the HL edge connection, the longitudinal length of the connection did not depict a high impact as that of the DS edge connection. The increment and decrement of the connector's length (comparison group 6) minorly improved the HL edge connection's load capacity by 5.56% and 3.54%, respectively. This is because the HL joint's flexural reaction was not only dependent on the CLT panel around the mid-span but was also related to the vertically jointed dowel connectors. Meanwhile, the change in connector length significantly decreased the ductility of the HL edge connection up to 19.62%, which implied that the HL edge connection with a longer distance was more ductile due to that the longer HL edge connection was looser than that of the others. Comparison group 7 illustrated that the load capacity of the HL edge connection had a positive correlation with the number of dowel connectors, which was improved up to 33.84%. The reason for this was that the dowel connection was the only joint that assembled the panels through the shear plane. Therefore, the increment of the dowel connectors increased the shear plane area, which directly reinforced the connection's shear strength. Based on this principle, the model with an increased number of dowels and different placement (2-480-2-3-45-240) also presented a large improvement in the load capacity, which was up to 55.05%. According to the displacements at failure seen with comparison groups 7 and 8, it was perceived that all the models' ductility decreased greatly (up to 8.49%). This meant that the stability of the HL edge connection was developed by adding more dowels. A possible explanation is that the increased number of dowels helped to distribute the transferred load at the horizontal plane more evenly. Therefore, the more dowels applied on the HL edge connection, the better the stability and bending capacity. Comparison group 9 studied the influence of the thickness of the half-thick panels at the mid-span, which showed that the thickness of the upper panel at the mid-span had an extremely positive correlation with the connection's ultimate load (up to 80.81%). Meanwhile, it also performed the lowest load capacity (0.35 kN) among the HL edge connection models when the thickness of the upper panel at the mid-span decreased by 30 mm (2-480-2-1-60-240). This is because the HL edge connection was point-jointed at the mid-span; therefore, the transferred load was majorly bored by the upper panel at the mid-span through bending. Based on the outcomes of comparison group 10, the longitudinal distance between the dowels and the edge of the upper panel positively affected the HL edge connection's load capacity and stability, which was improved up to 44.44% and 9.55%, respectively. This is because the lower part panel at the mid-span was not 100% activated for bending, and only the part between the dowels and the edge of the upper panel was activated. Therefore, the farther the dowels were located from the upper panel's edge, the longer the lower panel was activated. Hence, it is preferred to place the dowel connectors as far as from the upper panel's edge based on the perspective of the load capacity.

3.4. Load–Strain Performance

The obtained longitudinal strains from the nine strain collection points in all twenty numerical models were collected and are presented in Figure 8, as well as the ultimate load.

Based on the load–strain curves of the DS edge connection, it was observed that positions 1 and 3 have distinctly higher absolute values of strains than those of the other strain collection points. It indicated that the longitudinal layer on the top of the CLT panel was bearing a better part of the transferred load than other layers at the outer surface. This is because the DS edge connection mainly connected the transverse layer, where longitudinal layers of the connected CLT panels' bottom will split away from the mid-span without restraint. Meanwhile, the top longitudinal layer and transverse layer of the two connected CLT panels will attach and interact with each other under the out-of-plane bending. Among all the models of the DS edge connection, positions 1, 3, and 7, 9 displayed almost the same strain value throughout the loading process, as well as the load–strain relation. It implied that the internal stress on the longitudinal layers was symmetric based on the center point of the mid-span (positions 2 and 8). This phenomenon was caused due to the DS joints being placed symmetrically based on positions 2 and 8 as well. During the bending test, positions 1, 3, and 7, 9 received tension and compression, respectively. This outcome was not expected, and a typical CLT panel without connection normally receives compression and tension along the longitudinal direction on the CLT panel's top and bottom layers, respectively. The potential reasons for this difference were that (1) the DS edge connection cut off the grain at the CLT panel's mid-span, which affected the load transfer manner, too, and (2) the DS edge connection divided the mid-span line into three parts instead of along the entire mid-span's path, which created different constraint conditions for each part. Therefore, the strains' orientations also vary along the panel's top and bottom surfaces. For example, the center points of the mid-span (positions 2 and 8) depicted converse strain orientations (compression and tension, respectively) compared to those of the positions near positions 2 (positions 1 and 3) and 8 (positions 7 and 9). The strain values from positions 2 and 8 were generally smaller than those from positions 1, 3, and 7, 9 due to their different locations and constraint conditions. However, the strain of position 2 from the model '1-240-10-2-60-1—3' (Figure 8f) was significantly higher than that of the others, which exhibited almost the same value as that from positions 1 and 3 in the same model (but converse strain orientation). This phenomenon hinted that the increment of dowel numbers could improve the internal load distribution within the divided areas of the mid-span.

According to the load–strain diagrams of the ten HL edge connection models (Figure 9a–j), it was observed that the obtained longitudinal strains from most positions (1, 2, 3, 4, 6, 7, 8, and 9) were relatively lower than those of position 5. The results illustrated that the flexural behavior of the connected CLT panels was majorly dependent on the panel's transverse layer. This is because the geometry of the HL edge connection only fixed the connected CLT panels in the longitudinal direction through its transverse layers. Meanwhile, tension was witnessed from the transverse layer (position 5), which was expected, as the transverse layer's orientation was parallel to the CLT panel's major direction. Besides, positions 7–9 almost presented ignorable minor strains located on the bottom of the CLT panel's mid-span. This is because the lower part of the connection was assembled by the dowel connectors at its midpoint, where half of the lower connection (the part next to the lower connection's edge) was not receiving internal force due to no constraint on the boundary (lower panel's edge). Positions 1, 2, and 3 depicted relatively small amounts of strain (tension) among each other, which indicated that the CLT panel's top longitudinal layer was activated again by a small amount of internal force in an even manner. This was due to the HL edge connection being placed along the mid-span's full path. The models '2-240-2-1-45-240', '2-720-2-1-45-240', and '2-480-2-1-45-360' improved the distributed load in the HL edge connection's lower part after changing the connection's longitudinal length or the location of dowel connectors. This is because these modifications impacted the effective length of the connection's lower part (between the dowel connectors and the edge of the upper panel) against the internal load. The model '2-480-2-1-60-240' displayed uncommon load–strain curves compared to those of the other models, which appeared to have extremely small strains in all nine positions. A likely explanation for this phenomenon was that the generated internal force within the CLT panel at mid-span was ignorably

small, and the force concentrated in the dowel connectors. The thickness of the upper panel was increased to 60 mm in the model '2-480-2-1-30-240', and compression was noted from position 5, which is transverse compared to that of the others. This is because position 5 in the model '2-480-2-1-30-240' became part of the upper panel, but it still performed a similar absolute strain value as that of the other models. It represented that the transverse layer from both the upper and lower CLT panels bore a similar amount of internal force in opposite directions, which confirmed again that the transverse layer in the HL edge connection was taking a greater amount of transferred load than that of the longitudinal layers due to the geometry and degrees of freedom of the HL joint.

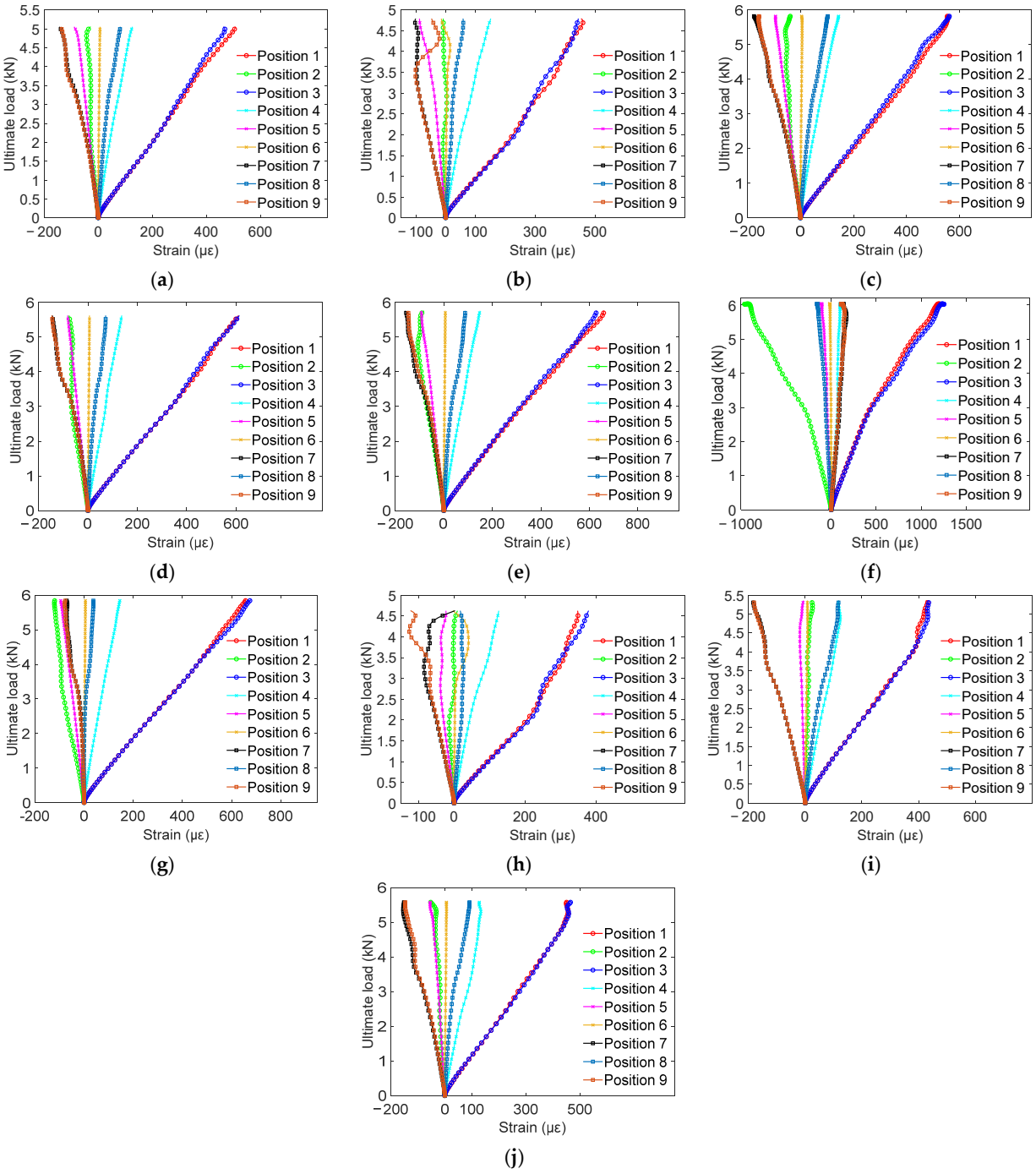

Figure 8. Load–strain diagrams under four-point bending test: (**a**) 1-240-10-1-60-1—3, (**b**) 1-120-10-1-60-1—3, (**c**) 1-360-10-1-60-1—3, (**d**) 1-240-15-1-60-1—3, (**e**) 1-240-20-1-60-1—3, (**f**) 1-240-10-2-60-1—3, (**g**) 1-240-10-2c-60-1—3, (**h**) 1-240-10-1-180-1—3, (**i**) 1-240-10-1-60-1—2, and (**j**) 1-240-10-1-60-2—3.

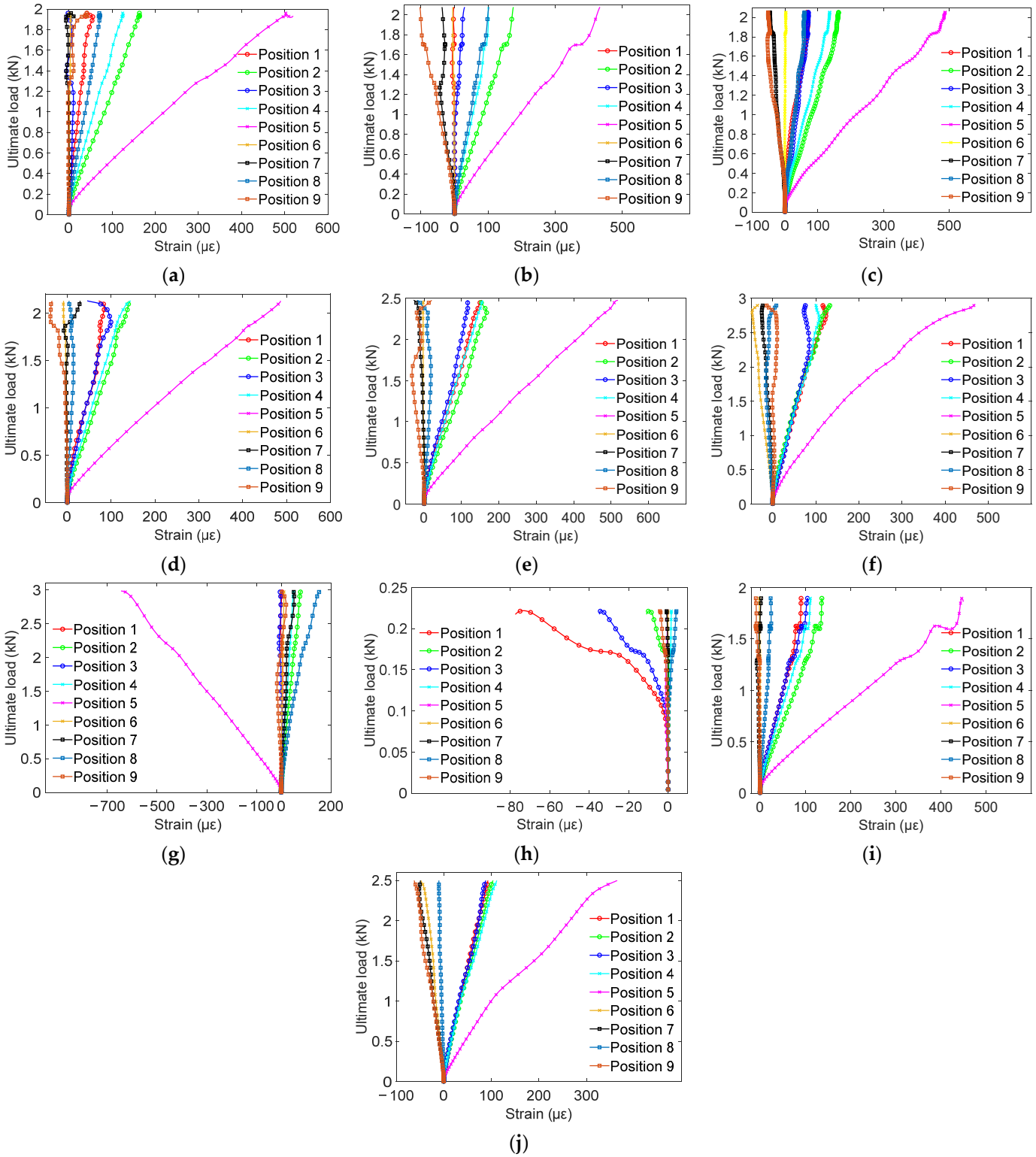

Figure 9. Load–strain diagrams under four-point bending test: (**a**) 2-480-2-1-45-240, (**b**) 2-240-2-1-45-240, (**c**) 2-720-2-1-45-240, (**d**) 2-480-3-1-45-240, (**e**) 2-480-4-1-45-240, (**f**) 2-480-2-3-45-240, (**g**) 2-480-2-1-30-240, (**h**) 2-480-2-1-60-240, (**i**) 2-480-2-1-45-120, and (**j**) 2-480-2-1-45-360.

3.5. Strain Distribution along the Mid-Span Depth

Figure 10 presents the strain distribution over the CLT panel's mid-span depth in all the models of the DS and the HL edge connections, which were collected from positions 4, 5, and 6. Besides, the strains from these positions under different levels of loaded force were also extracted and compared within each numerical model. Based on the CLT panel's height versus strain graphs of the DS edge connection, it was witnessed that the strain majorly occurred in the area above the panel depth's midpoint (positions 4 and 5). The CLT panel's bottom area exhibited nearly zero strain of the entire bending process among all models with the DS connection. This was due to the fact that the bottom edge of the CLT panel's mid-span lacked joints, which could prevent the mid-span's bottom edges from splitting in different directions. The numbers and location change of the dowel connector ('1-240-10-2-60-1—3' and '1-240-10-1-180-1—3') slightly improved the internal force at the mid-span's bottom edge because these two parameters could improve the DS joint's tightness. Meanwhile, those two parameters also showed a greater improvement in the strains in positions 4 and 5. The results from position 6 of all comparison models also implied that the load efficiency on the bottom longitudinal layer was difficult to improve under the DS edge connection compared to that of the transverse and top longitudinal layers. As for the strain distributions from positions 4 and 5, a good linear relationship was observed between them, where compression and tension were found from positions 5 and 4, respectively. Meanwhile, the strain's absolute value from position 4 was relatively higher than that of position 5 because the CLT's edges with the DS joint were more tightly attached to each other on the top longitudinal layer than that of the transverse layer. The strains of the transverse layer from the models '1-240-10-1-60-1—2' and '1-240-10-1-60-2—3' were evidently decreased compared to those of the others. It meant that the decrease in the dowel connector's length had negatively affected the internal force at the transverse layer. However, the modification of the dowel's length did not impact the strain of the top longitudinal layer (position 4) because it was majorly activated by the internal tensile force from the CLT panel instead of from the dowel connectors.

The strain distribution over the mid-span height from the HL edge connection (Figure 11a–j) displayed different patterns from that of the DS edge connection. This is because positions 4, 5, and 6 from the DS edge connection were extracted from the same panel (half of the connected CLT panel), while that of the HL edge connection was extracted from different parts of the connected CLT panel. Based on the models with the HL edge connection, position 5 also depicted nearly zero strain in most of the models due to a lack of boundary constraint on the bottom layer, which was like that of the DS edge connection. According to the results of the HL edge connection, positions 4 and 5 all exhibited different amounts of tensile deformation, where the former was relatively smaller than the latter. This was due to both positions belonging to the same CLT panel (upper panel) before it was connected to another panel, and position 5 was from the transverse layer that bore the major part of the internal force. Most of the models with the HL joints had similar strain patterns except for two models, '2-480-2-1-30-240' and '2-480-2-1-60-240', where the former showed compression, and the latter obtained barely zero strain within positions 4, 5, and 6. This was because the thickness of the upper and lower HL connections had been modified, which directly influenced the internal load's orientation in position 5.

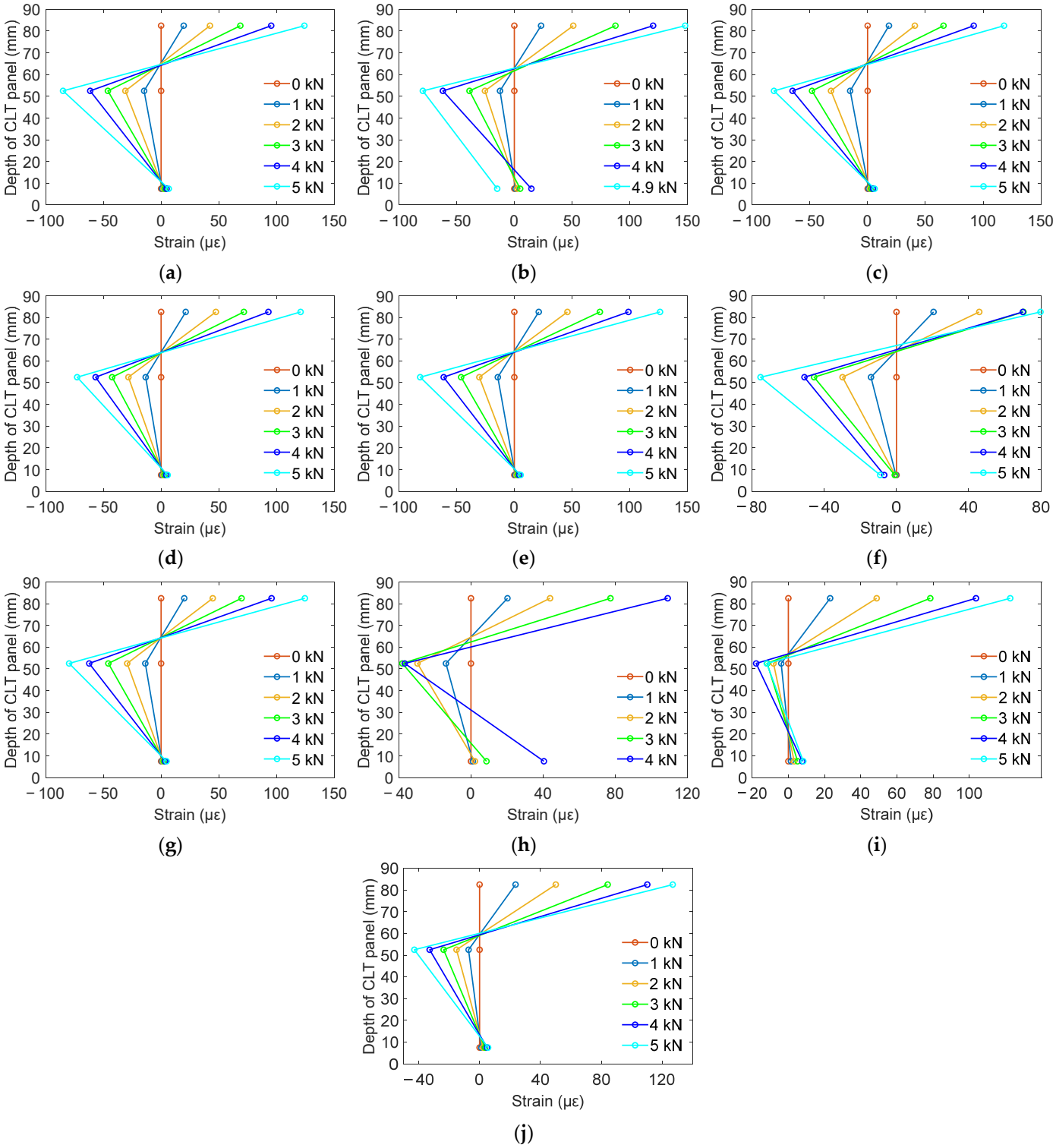

Figure 10. Strain distribution over connected CLT panel's height at mid-span: (**a**) 1-240-10-1-60-1—3, (**b**) 1-120-10-1-60-1—3, (**c**) 1-360-10-1-60-1—3, (**d**) 1-240-15-1-60-1—3, (**e**) 1-240-20-1-60-1—3, (**f**) 1-240-10-2-60-1—3, (**g**) 1-240-10-2c-60-1—3, (**h**) 1-240-10-1-180-1—3, (**i**) 1-240-10-1-60-1—2, and (**j**) 1-240-10-1-60-2—3.

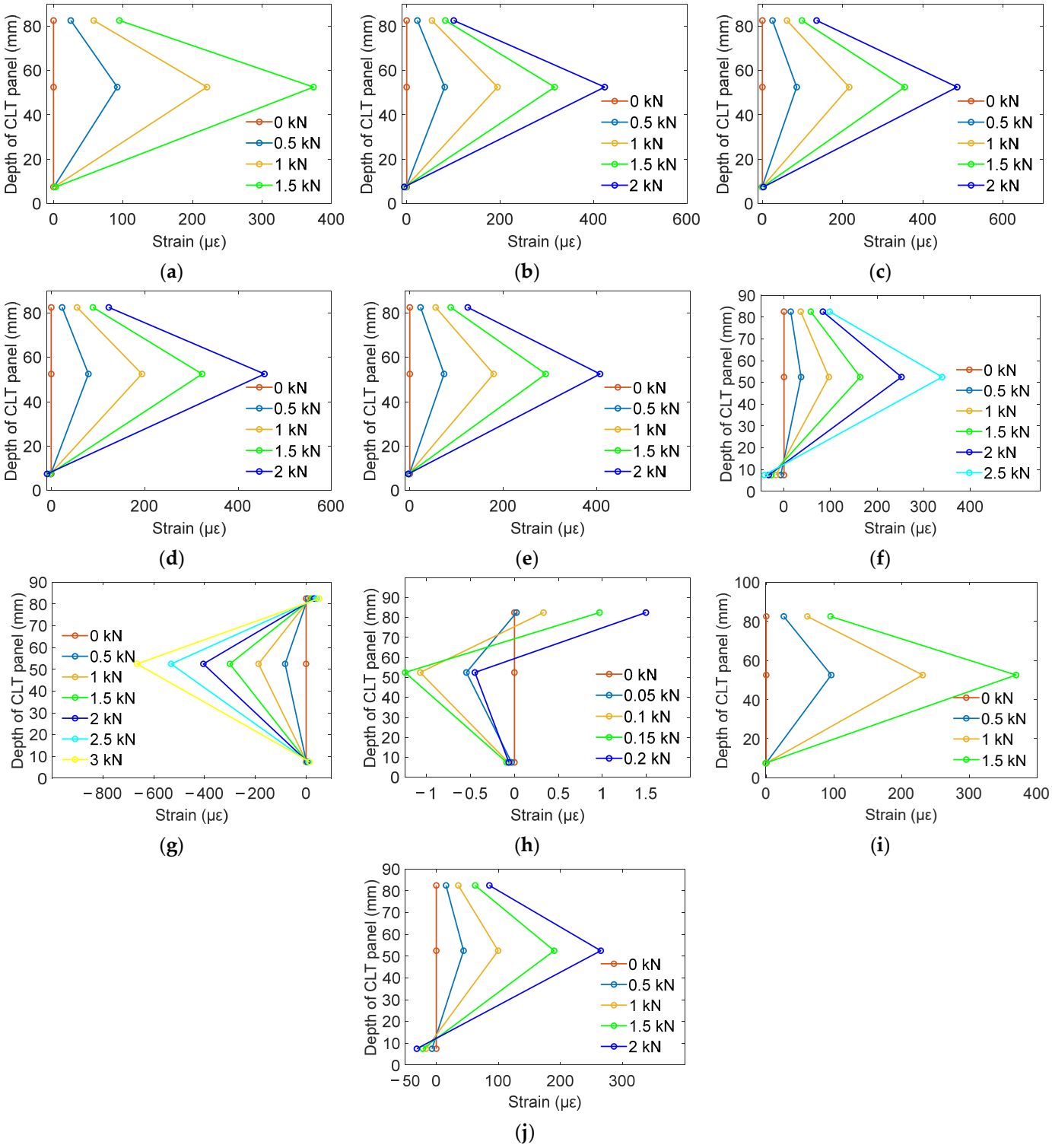

Figure 11. Strain distribution over connected CLT panel's height at mid-span: (**a**) 2-480-2-1-45-240, (**b**) 2-240-2-1-45-240, (**c**) 2-720-2-1-45-240, (**d**) 2-480-3-1-45-240, (**e**) 2-480-4-1-45-240, (**f**) 2-480-2-3-45-240, (**g**) 2-480-2-1-30-240, (**h**) 2-480-2-1-60-240, (**i**) 2-480-2-1-45-120, and (**j**) 2-480-2-1-45-360.

3.6. Stress Distribution, Failure Modes, and Deflection Distribution

The von Mises stress distributions (MPa) of all studied numerical models are presented in Figure 12, as well as their failure modes. It was perceived that the stress distributions from the CLT panels with the DS edge connection were asymmetric based on the mid-span path, which generally existed on (1) part of the top longitudinal layer between the two load sets, (2) a major part of the transverse layer, (3) all dowel connectors, and (4) part of the bottom lamella layer that was nearby the dowel connectors. Meanwhile, the main stress came from the dowel connectors, the mid-span edge, and the transverse layers, which were adjacent to the load sets. This was because the DS connection joined the transverse layers by two boundaries, which were the mid-span edge and the dowel connector. Among the models with the DS edge connection, the stress distribution on the longitudinal was not evenly distributed along the longitudinal layers. Instead, high stress occurred around the rectangular and dowel connectors. Then, the stress gradually reduced as the distance from the connector became longer. The reason for this phenomenon was that the DS edge connection was partially placed on the mid-span edge, where the initial and primary rotation moments were generated from the rectangular connectors. Therefore, the stress surrounding the dowel connectors was decreased effectively when the dowel connector's number increased ('1-240-10-2-60-1—3' and '1-240-10-2c-60-1—3') due to the changes in the boundary condition of the rectangular connectors. As for the panels with the HL edge connection (Figure 12k–t), the stress generally appeared in three areas throughout the entire panel width as follows: (1) on the top surface of the upper panel under the right-side load set, (2) on the bottom surface under the left-side load set, (3) the bottom surface of the upper panel between the dowel connectors and the right-side load set, and (4) the dowel connectors. The failures primarily happened at the dowel connections when the models included only two dowels. The reason for this was that the dowel connectors were damaged by the internal force from the HL edge connection before it crashed the panel's other parts (the half-lapped area and the panel's outer surfaces). It indicated that the strength of two dowel connectors was insufficient for making the HL connection efficiently work with the default parameters. This issue had been improved in the models '2-480-3-1-45-240', '2-480-4-1-45-240', and '2-480-2-3-45-240', where the internal force was more concentrated on the CLT panels between the two load sets.

Figure 13 provides the ultimate deflection distributions of two deformed numerical models, '1-240-10-1-60-1—3' and '2-480-2-1-45-240'. It was seen that the panel with a DS edge connection showed symmetrical deflection along the longitudinal direction based on the mid-span edge. A similar performance was also perceived on the panel with the HL edge connection, except for the bottom layer between the load sets. Therefore, the maximum deflection of the model with the HL edge connection on the Z-direction was obtained from the lower panel's edge instead of the connected panel's midpoint (1-240-10-1-60-1—3). This was because the half-lapped part of the lower panel was not constrained by its edge, which also indicated that this part was barely deformed. Among those two models, the panels' deflections from the load set to the supports were linearly decreased, which was expected because the panels' two outer sides were fixed against the Z-direction.

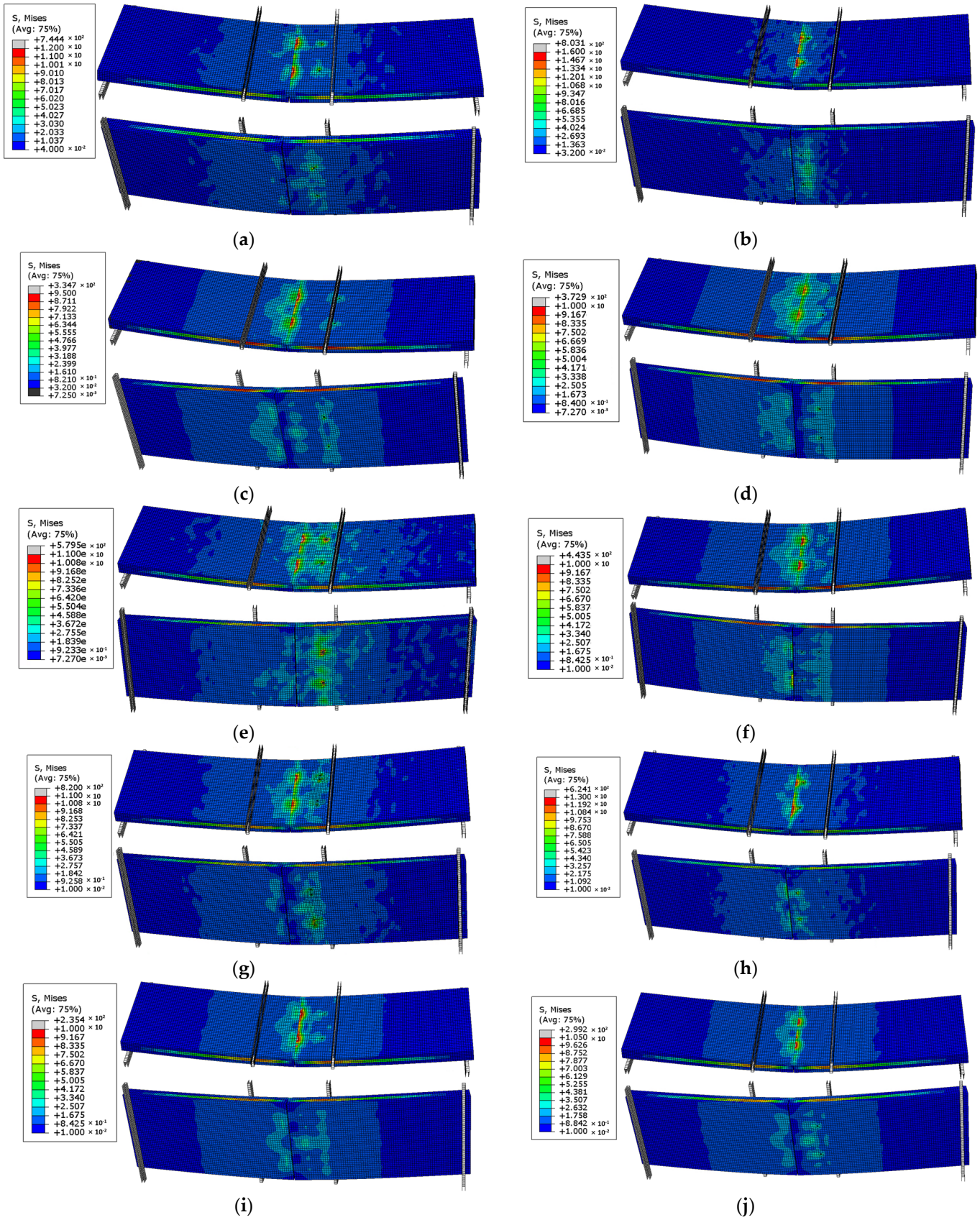

Figure 12. *Cont.*

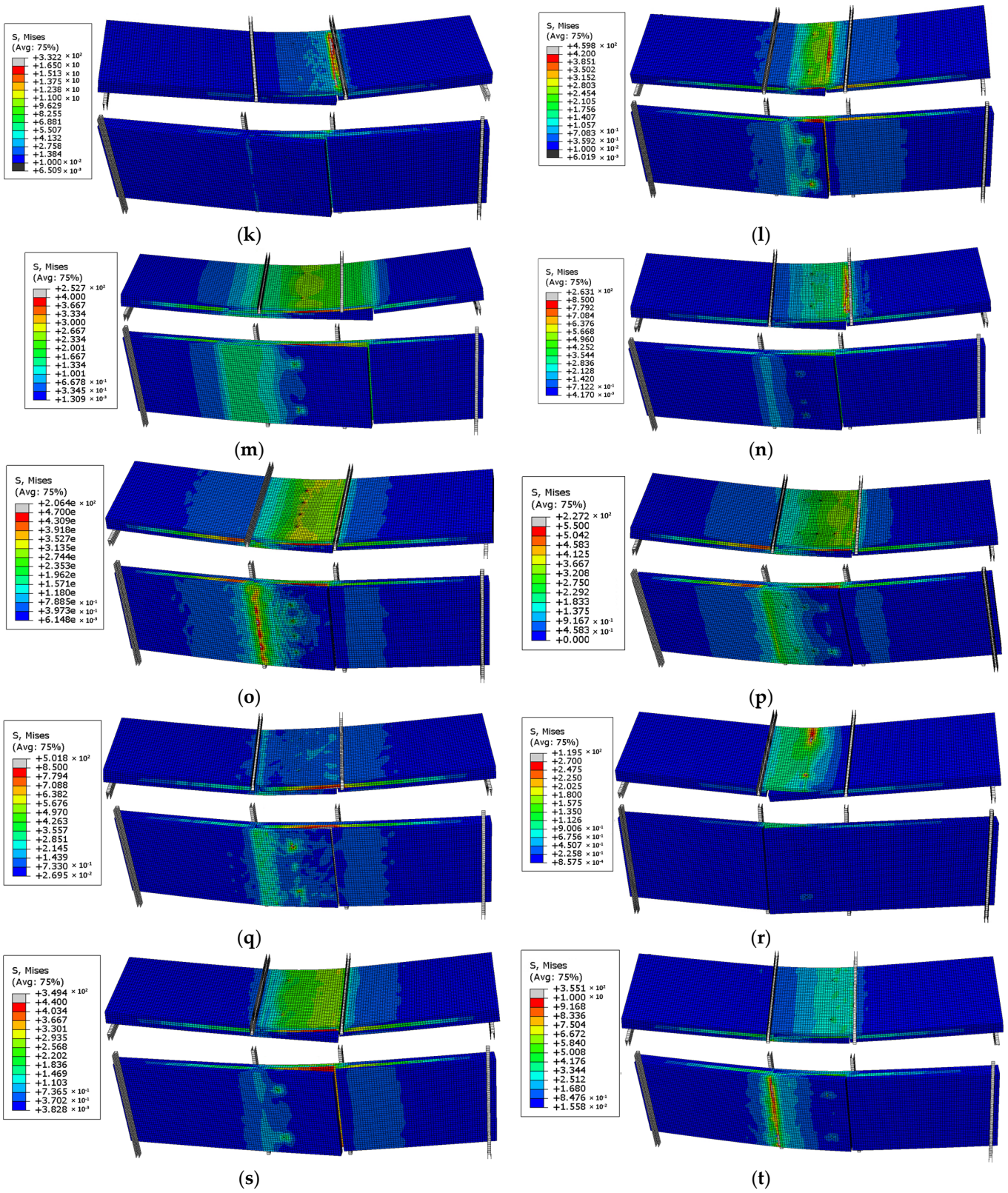

Figure 12. Contours of von Mises stress and failure mode for CLT panels with DS or HL edge connections: (**a**) 1-240-10-1-60-1—3, (**b**) 1-120-10-1-60-1—3, (**c**) 1-360-10-1-60-1—3, (**d**) 1-240-15-1-60-1—3, (**e**) 1-240-20-1-60-1—3, (**f**) 1-240-10-2-60-1—3, (**g**) 1-240-10-2c-60-1—3, (**h**) 1-240-10-1-180-1—3, (**i**) 1-240-10-1-60-1—2, (**j**) 1-240-10-1-60-2—3, (**k**) 2-480-2-1-45-240, (**l**) 2-240-2-1-45-240, (**m**) 2-720-2-1-45-240, (**n**) 2-480-3-1-45-240, (**o**) 2-480-4-1-45-240, (**p**) 2-480-2-3-45-240, (**q**) 2-480-2-1-30-240, (**r**) 2-480-2-1-60-240, (**s**) 2-480-2-1-45-120, and (**t**) 2-480-2-1-45-360 (units are in MPa).

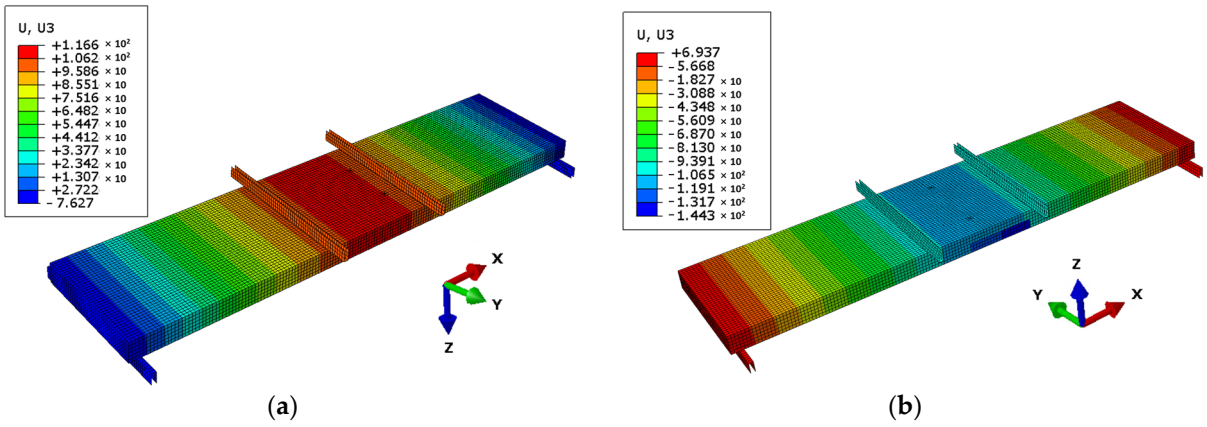

(**a**) (**b**)

Figure 13. Deflection distribution of CLT panels with DS and HL edge connections: (**a**) 1-240-10-1-60-1—3 and (**b**) 2-480-2-1-45-240 (units are in mm).

4. Conclusions and Recommendations

In the current study, two innovative adhesive-free timber edge connections (the DS and the HL connections) for CLT panels were proposed to reinforce CLT's structural integrity and minimize the use of adhesive for environmental consideration. Twenty parametric models based on the DS and the HL edge connections were conducted numerically under the four-point bending test. The studied parameters include the connection's length and thickness, the connector's number, the placement of the connector, and the integrated lamella layers. The findings and analyses of the parametric studies are summarized as follows:

- The models concerned with the DS and the HL edge connections exhibited the ultimate load ranges of 4.95–6.23 kN and 0.35–3.58 kN, respectively, with the mean load capacity of the DS edge connection at 5.70 kN, which was 149% higher than 2.29 kN of the HL edge connection.
- The preferred 15 mm diameter dowel connections in the DS edge connection improved the load capacity by 15.26%, while increments in the horizontal length of the DS connection and adjustments in the placement of its dowel connectors raised the CLT panel's ultimate load by 8.8% and 8.83%, respectively.
- The CLT panels that utilized the HL edge connections were generally more ductile but less stable, with greater load capacity standard deviations, compared to those with the DS edge connections, which demonstrated both the tensile and compressive failures, whereas the panels with the HL edge connections mostly failed due to the tension.
- The number of dowel connections from both the DS and the HL edge connections positively correlated with their load capacities (up to 11.71% and 80.81%, respectively).
- Factor 'd' played an important role in the panel's ultimate load (an improvement of 44.44% by increasing 'd') regarding the HL connection. Meanwhile, the panels with the DS edge connection were minorly impacted by the factor 'd'.
- The load capacity of the panels with the HL edge connection was improved by 80.81% due to the increment of the connection's upper thickness. The recommended thickness of the HL connection's upper thickness should be above 45 mm at least.
- Stress and deformation barely existed at most of the panels' bottom lamella layers. This situation can be improved by (1) increasing the number of dowl connectors and (2) modifying the dowel connectors' location.
- According to the validation of the numerical model, the developed numerical models (31.96 kN and 87.1 mm) exhibited a slightly lower load capacity (−0.1%) and a greater deflection at failure (1.9%) than that of the experimental tests' mean values (32 kN and 85.4 mm).

Based on the summarized results, it can be concluded that adhesive-free timber edge connections could substitute adhesives and metallic fasteners from the perspective of

load capacity. A preferable flexural behavior could be obtained by modifying some of the connections' parameters (such as the connector's dimensions, location, and number). The current study's limitations include the following: (1) the research outcomes only apply to the static bending performance, and (2) the investigation covered connections for CLT panels only. Future investigations will focus on optimizing the studied connections and continue to examine new connections, considering structural performance, energy efficiency, and environmental impact. Meanwhile, studies on applying edge connections between wall-to-wall and wall-to-floor are also needed.

Author Contributions: Conceptualization, H.R. and A.B.; methodology, H.R. and A.B.; software, H.R.; validation, H.R. and A.B.; formal analysis, H.R. and A.B.; investigation, H.R. and A.B.; data curation, H.R. and A.B.; writing—original draft preparation, H.R.; writing—review and editing, H.R., A.B., M.C. and M.W.; visualization, H.R. and A.B.; supervision, A.B., M.C. and M.W. All authors have read and agreed to the published version of the manuscript.

Funding: This research received no external funding.

Data Availability Statement: The data that support the findings of this study are available from the corresponding author upon reasonable request.

Acknowledgments: The authors are thankful to the University of Gävle for funding this research work.

Conflicts of Interest: The authors declare no conflicts of interest.

References

1. Grebner, D.L.; Bettinger, P.; Siry, J.P.; Boston, K. Forest Products. In *Introduction to Forestry and Natural Resources*; Academic Press: Cambridge, MA, USA, 2022; pp. 101–129. [CrossRef]
2. Xin, Z.; Gattas, J. Structural Behaviors of Integrally-Jointed Plywood Columns with Knot Defects. *Int. J. Struct. Stab. Dyn.* **2021**, *21*, 2150022. [CrossRef]
3. Jockwer, R.; Brühl, F.; Cabrero, J.M.; Hübner, U.; Leijten, A.; Munch-Anderssen, J.; Ranasinghe, K. Modern Connections in the Future Eurocode 5—Overview of Current Developments. In Proceedings of the World Conference on Timber Engineering 2021, WCTE 2021, Santiago, Chile, 9–12 August 2021.
4. Harley, T.; White, G.; Dowdall, A.; Bawcombe, J.; McRobie, A.; Steinke, R. Dalston Lane—The World's Tallest CLT Building. In Proceedings of the WCTE 2016—World Conference on Timber Engineering, Vienna, Austria, 22–25 August 2016.
5. Tannert, T. Improved Performance of Reinforced Rounded Dovetail Joints. *Constr. Build. Mater.* **2016**, *118*, 262–267. [CrossRef]
6. Techlam, N.Z. Advantages & Benefits of Glulam. Available online: https://techlam.nz/about/advantages-benefits-of-glulam/ (accessed on 20 November 2023).
7. Zhang, Y.; Zhang, X.; Wang, L. Experimental Validation and Simplified Design of an Energy-Based Time Equivalent Method Applied to Evaluate the Fire Resistance of the Glulam Exposed to Parametric Fire. *Eng. Struct.* **2022**, *272*, 115051. [CrossRef]
8. Bahrami, A.; Vall, A.; Khalaf, A. Comparison of Cross-Laminated Timber and Reinforced Concrete Floors with Regard to Load-Bearing Properties. *Civ. Eng. Archit.* **2021**, *9*, 1395–1408. [CrossRef]
9. Bahrami, A.; Edås, M.; Magnenat, K.; Norén, J. The Behavior of Cross-Laminated Timber and Reinforced Concrete Floors in a Multi-Story Building. *Int. J. Adv. Appl. Sci.* **2022**, *9*, 43–50. [CrossRef]
10. Bahrami, A.; Nexén, O.; Jonsson, J. Comparing Performance of Cross-Laminated Timber and Reinforced Concrete Walls. *Int. J. Appl. Mech. Eng.* **2021**, *26*, 28–43. [CrossRef]
11. Bajzecerová, V.; Kanócz, J.; Rovňák, M.; Kováč, M. Prestressed CLT-Concrete Composite Panels with Adhesive Shear Connection. *J. Build. Eng.* **2022**, *56*, 104785. [CrossRef]
12. Wang, M.; Xu, Q.; Harries, K.A.; Chen, L.; Wang, Z.; Chen, X. Experimental Study on Mechanical Performance of Shear Connections in CLT-Concrete Composite Floor. *Eng. Struct.* **2022**, *269*, 114842. [CrossRef]
13. Jeong, G.Y.; Pham, V.S.; Tran, D.K. Development of Predicting Equations for Slip Modulus and Shear Capacity of CLT–Concrete Composite with Screw Connections. *J. Build. Eng.* **2023**, *71*, 106468. [CrossRef]
14. Xu, Q.; Wang, M.; Chen, L.; Harries, K.A.; Song, X.; Wang, Z. Mechanical Performance of Notched Shear Connections in CLT-Concrete Composite Floor. *J. Build. Eng.* **2023**, *70*, 106364. [CrossRef]
15. Cao, J.; Xiong, H.; Wang, Z.; Chen, J. Mechanical Characteristics and Analytical Model of CLT-Concrete Compo-site Connections under Monotonic Loading. *Constr. Build. Mater.* **2022**, *335*, 127472. [CrossRef]
16. Asselstine, J.; Lam, F.; Zhang, C. New Edge Connection Technology for Cross Laminated Timber (CLT) Floor Slabs Promoting Two-Way Action. *Eng. Struct.* **2021**, *233*, 111777. [CrossRef]
17. Tapia, C.; Claus, M.; Aicher, S. A Finger-Joint Based Edge Connection for the Weak Direction of CLT Plates. *Constr. Build. Mater.* **2022**, *340*, 127645. [CrossRef]

18. Khai Tran, D.; Young Jeong, G. Tension Resistance Properties of Hold-down and Angle-Bracket Connections on Cross-Laminated Timber (CLT). *Structures* **2023**, *56*, 104841. [CrossRef]
19. Zhang, J.; Zhang, C.; Li, Y.; Chang, W.S.; Huang, H. Cross-Laminated Timber (CLT) Floor Serviceability under Multi-Person Loading: Impact of Beam–Panel Connections. *Eng. Struct.* **2023**, *296*, 116941. [CrossRef]
20. Udele, K.E.; Sinha, A.; Morrell, J.J. Effects of Re-Drying on Properties of Cross Laminated Timber (CLT) Connections. *J. Build. Eng.* **2023**, *76*, 107298. [CrossRef]
21. Milojević, M.; Racic, V.; Marjanović, M.; Nefovska-Danilović, M. Influence of Inter-Panel Connections on Vibration Response of CLT Floors Due to Pedestrian-Induced Loading. *Eng. Struct.* **2023**, *277*, 115432. [CrossRef]
22. Khai Tran, D.; Jeong, G.Y. Design of Geometric Variables of Hold-down and Angle Bracket Connections for Lateral Resistance Enhancement of Cross-Laminated Timber (CLT) Walls Considering the Influence of Wood Species, Load-Grain Angles, and Floor Conditions. *Structures* **2023**, *48*, 1003–1017. [CrossRef]
23. Aloisio, A.; De Santis, Y.; Pasca, D.P.; Fragiacomo, M.; Tomasi, R. Aleatoric and Epistemic Uncertainty in the Overstrength of CLT-to-CLT Screwed Connections. *Eng. Struct.* **2024**, *304*, 117575. [CrossRef]
24. Hemmilä, V.; Adamopoulos, S.; Karlsson, O.; Kumar, A. Development of Sustainable Bio-Adhesives for Engineered Wood Panels-A Review. *RSC Adv.* **2017**, *7*, 38604–38630. [CrossRef]
25. Stark, N.M.; Cai, Z.; Carll, C. Wood-Based Composite Materials: Panel Products, Glued-Laminated Timber, Structural Composite Lumber, and Wood-Nonwood Composite Materials. In *General Technical Report FPL–GTR–190*; Forest Products Laboratory (US): Madison, WI, USA, 2010.
26. Qiao, G.; Li, T.; Frank Chen, Y. Assessment and Retrofitting Solutions for an Historical Wooden Pavilion in China. *Constr Build Mater* **2016**, *105*, 435–447. [CrossRef]
27. Crowther, P. Historic Trends in Building Assembly. In Proceedings of the ACSA/CIB International Science and Technology Conference—Technology in Transition: Mastering the Impacts, Montreal, QC, Canada, 25–29 June 1999.
28. Baño, V.; Moltini, G. Experimental and Numerical Analysis of Novel Adhesive-Free Structural Floor Panels (TTP) Manufactured from Timber-to-Timber Joints. *J. Build. Eng.* **2021**, *35*, 102065. [CrossRef]
29. Ilgın, H.E.; Karjalainen, M.; Alanen, M.; Malaska, M. Evaluating Fire Performance: An Experimental Comparison of Dovetail Massive Wooden Board Elements and Cross-Laminated Timber. *Fire* **2023**, *6*, 352. [CrossRef]
30. Sotayo, A.; Bradley, D.; Bather, M.; Sareh, P.; Oudjene, M.; El-Houjeyri, I.; Harte, A.M.; Mehra, S.; O'Ceallaigh, C.; Haller, P.; et al. Review of State of the Art of Dowel Laminated Timber Members and Densified Wood Materials as Sustainable Engineered Wood Products for Construction and Building Applications. *Dev. Built Environ.* **2020**, *1*, 100004. [CrossRef]
31. Structure Craft. Dowel Laminated Timber—The All Wood Panel—Mass Timber Design Guide. Available online: https://structurecraft.com/blog/dowel-laminated-timber-design-guide-and-profile-handbook (accessed on 31 January 2024).
32. Vilguts, A.; Phillips, A.R.; Jerves, R.; Antonopoulos, C.; Griechen, D. Monotonic Testing of Single Shear-Plane CLT-to-CLT Joint with Hardwood Dowels. *J. Build. Eng.* **2024**, *88*, 109252. [CrossRef]
33. Mehra, S.; O'Ceallaigh, C.; Sotayo, A.; Guan, Z.; Harte, A.M. Experimental Characterisation of the Moment-Rotation Behaviour of Beam-Beam Connections Using Compressed Wood Connectors. *Eng. Struct.* **2021**, *247*, 113132. [CrossRef]
34. Mehra, S.; O'Ceallaigh, C.; Hamid-Lakzaeian, F.; Guan, Z.; Harte, A.M. Evaluation of the Structural Behaviour of Beam-Beam Connection Systems Using Compressed Wood Dowels and Plates. In Proceedings of the WCTE 2018—World Conference on Timber Engineering, Seoul, Republic of Korea, 20–23 August 2018.
35. Sotayo, A.; Bradley, D.F.; Bather, M.; Oudjene, M.; El-Houjeyri, I.; Guan, Z. Development and Structural Behaviour of Adhesive Free Laminated Timber Beams and Cross Laminated Panels. *Constr. Build. Mater.* **2020**, *259*, 119821. [CrossRef]
36. CEN. *EN 16351*; Timber Structures—Cross Laminated Timber—Requirements. Comit'e Europ´een de Normalisation: Brussels, Belgium, 2021.
37. CEN. *EN 1995-1-1*; Eurocode 5: Design of Timber Structures—Part 1-1: General—Common Rules and Rules for Buildings. Comit´e Europ´een de Normalisation: Brussels, Belgium, 2005.
38. Sitnikova, E.; Guan, Z.W.; Schleyer, G.K.; Cantwell, W.J. Modelling of Perforation Failure in Fibre Metal Laminates Subjected to High Impulsive Blast Loading. *Int. J. Solids Struct.* **2014**, *51*, 3135–3146. [CrossRef]
39. Gama, B.A.; Gillespie, J.W. Finite Element Modeling of Impact, Damage Evolution and Penetration of Thick-Section Composites. *Int. J. Impact Eng.* **2011**, *38*, 181–197. [CrossRef]
40. Hashin, Z. Failure Criteria for Unidirectional Fiber Composites. *J. Appl. Mech.* **1980**, *47*, 329–334. [CrossRef]